Reduced hematopoietic stem cell frequency predicts outcome in acute myeloid leukemia

Wenwen Wang,[1,8] Thomas Stiehl,[2] Simon Raffel,[1,3,4] Van T. Hoang,[1,9] Isabel Hoffmann,[1] Laura Poisa-Beiro,[1] Borhan R. Saeed,[1] Rachel Blume,[1] Linda Manta,[1] Volker Eckstein,[1] Tilmann Bochtler,[1,5] Patrick Wuchter,[1,10] Marieke Essers,[3,4] Anna Jauch,[6] Andreas Trumpp,[3,4,7] Anna Marciniak-Czochra,[2] Anthony D. Ho[1] and Christoph Lutz[1,7]

[1]Department of Medicine V, Heidelberg University, Germany; [2]Institute of Applied Mathematics, Interdisciplinary Center for Scientific Computing (IWR), BIOQUANT, Heidelberg University, Germany; [3]Division of Stem Cells and Cancer, Deutsches Krebsforschungszentrum (DKFZ), Heidelberg, Germany; [4]Heidelberg Institute for Stem Cell Technology and Experimental Medicine (HI-STEM gGmbH), Germany; [5]Clinical Cooperation Unit Molecular Hematology/Oncology, Deutsches Krebsforschungszentrum (DKFZ), Heidelberg, Germany; [6]Institute of Human Genetics, Heidelberg University, Germany; [7]German Cancer Consortium (DKTK), Heidelberg, Germany; [8]Present Address: Department of Oncology, Nanjing Medical University Affiliated Wuxi Second Hospital, Jiangsu, China; [9]Present Address: Georg-Speyer-Haus, Institute for Tumor Biology and Experimental Therapy, Frankfurt am Main, Germany and [10]Present Address: Institute of Transfusion Medicine and Immunology, Medical Faculty Mannheim, Heidelberg University; German Red Cross Blood Service Baden-Württemberg – Hessen, Germany

 doi:10.3324/haematol.2016.163584

Received: January 5, 2017.

Accepted: May 17, 2017.

Pre-published: May 26, 2017.

Correspondence: christoph.lutz@med.uni-heidelberg.de

Supplementary Figures

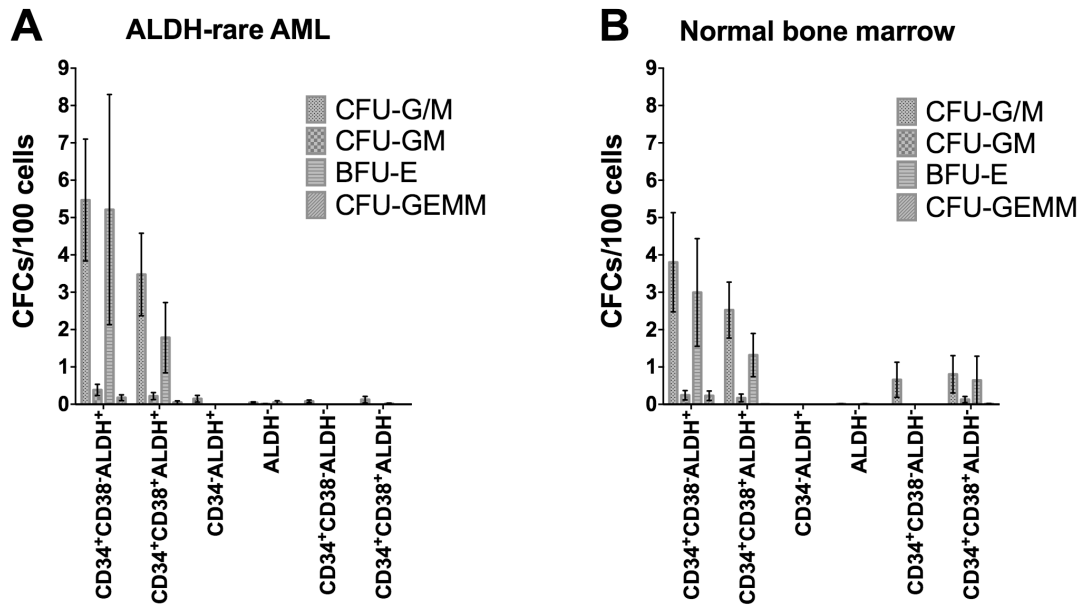

Figure S1: $CD34^+CD38^-ALDH^+$ cells show increased colony forming potential.

Comparison of CFC frequencies of different subpopulations derived from (A) ALDH-rare AML (n=25) and (B) normal BM (n=8). Data are shown as mean ± SEM.

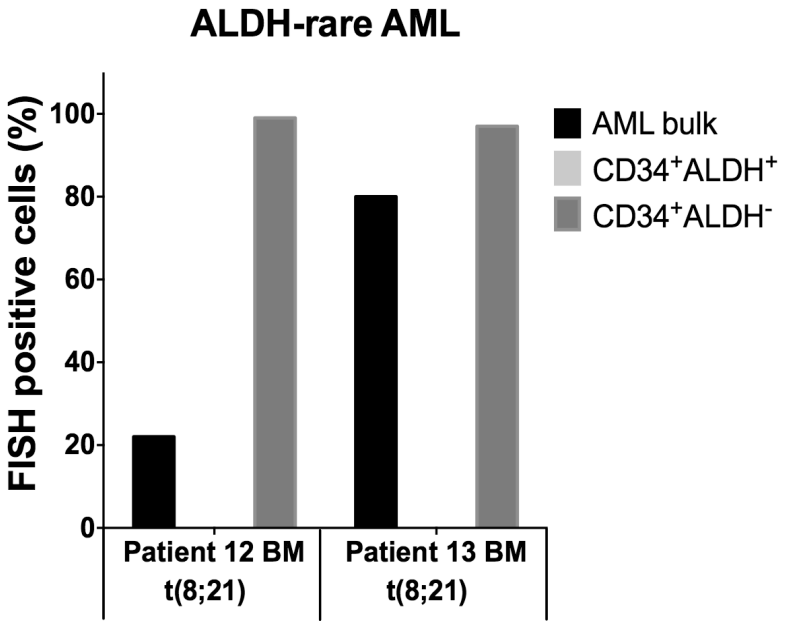

Figure S2: CD34^{+}ALDH^{+} cells are clonal marker negative.

FISH analysis shows clonal marker negativity for CD34^{+}ALDH^{+} cells of AML12,13.

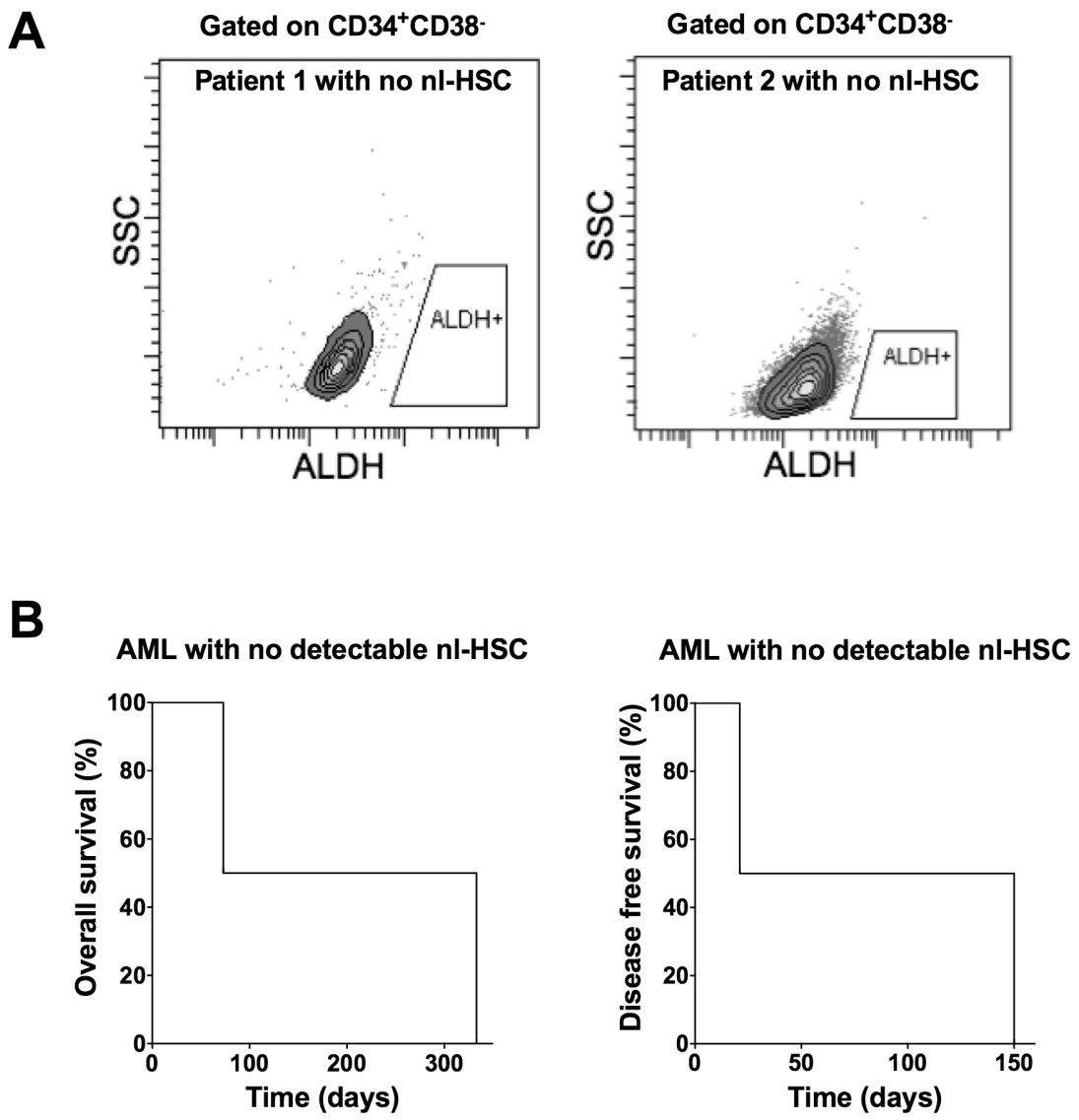

Figure S3: Patients with no detectable nl-HSC display extremely poor survival.

(A) FACS plots of 2 patients in which no $CD34^{+}CD38^{-}ALDH^{+}$ cells were detectable. (B) Survival analysis of 2 patients with no detectable nl-HSC revealed extremely poor overall and disease free survival.

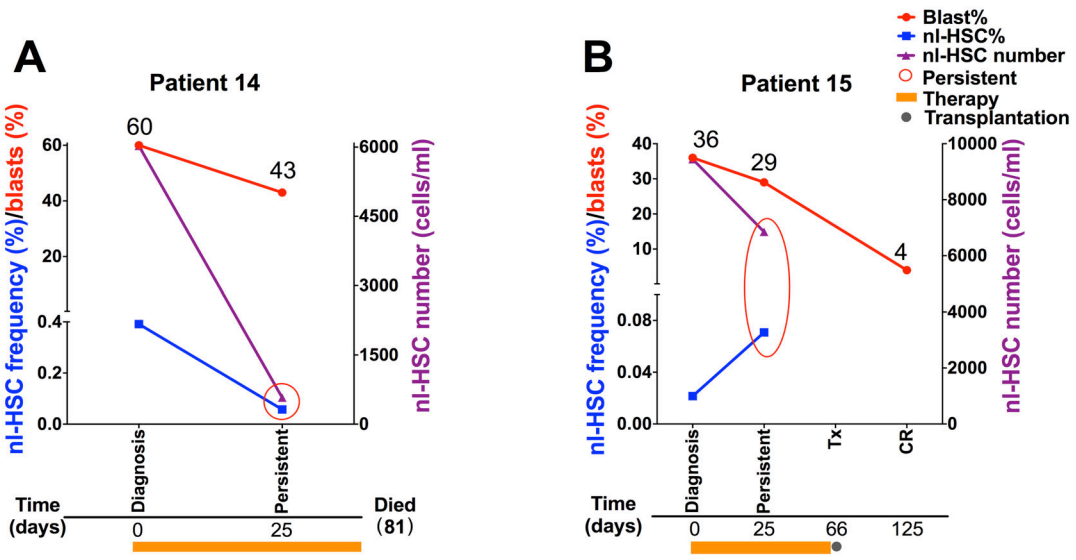

Figure S4: Residual nl-HSC decrease in AML cases with persistent disease.

Blast percentages and nl-HSC percentages at diagnosis and various follow-up time points with the percentage contribution of these populations in total BM MNC are shown for patients 14 and 15 (AB). Nl-HSC numbers are shown as cells/ml. Time points of persistence and the event of allogeneic HSCT are indicated on the respective time line. Detailed patient characteristics on this and other AML patients are described in Supplementary Table S2. CR (complete remission): blast% <5%; PR (partial remission): blast% 5-25%; Persistent: blast% >25%; Relapse: blast% ≥5%.

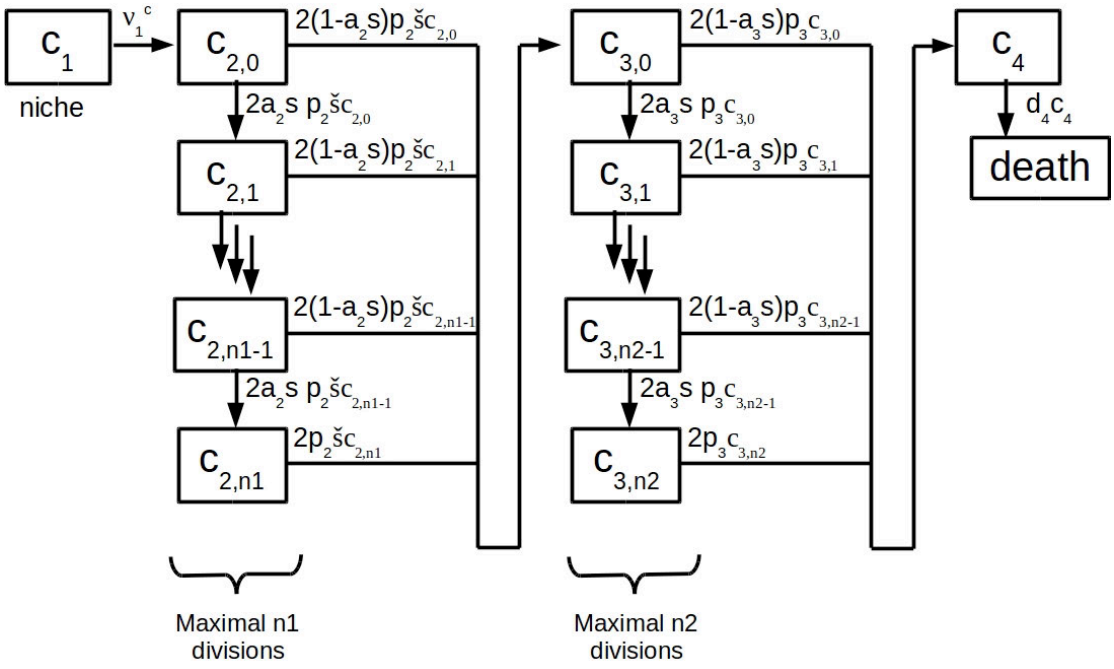

Figure S5: Model of the hematopoietic cell lineage.

Stem cells can divide infinitely. The maximal number of divisions a cell can perform in the progenitor or precursor state is limited by n_1 or n_2 respectively. Depending on environmental signaling, progenitors and precursors can differentiate before they have performed the maximal number of n_1 (n_2) divisions. c_1 : stem cells residing in the niche, $c_{2,0}$: progenitor cells that have performed 0 divisions since entrance into the progenitor state, $c_{2,1}$: progenitor cells that have performed 1 division since entrance into the progenitor state, etc. $c_{3,0}$: precursor cells that have performed 0 divisions since entrance into the progenitor state, $c_{3,1}$: precursor cells that have performed 1 division since entrance into the progenitor state, etc. c_4: mature cells. The respective proliferation rates are denoted as p_i, the fractions of self-renewal as a_i. The feedback signal regulating self-renewal is denoted as s, the feedback signal regulating proliferation rates of stem and progenitor cells as $\check{s}$. ν_1^c: flux from the stem cell compartment to the progenitor compartment, d_4: death rate of mature cells.

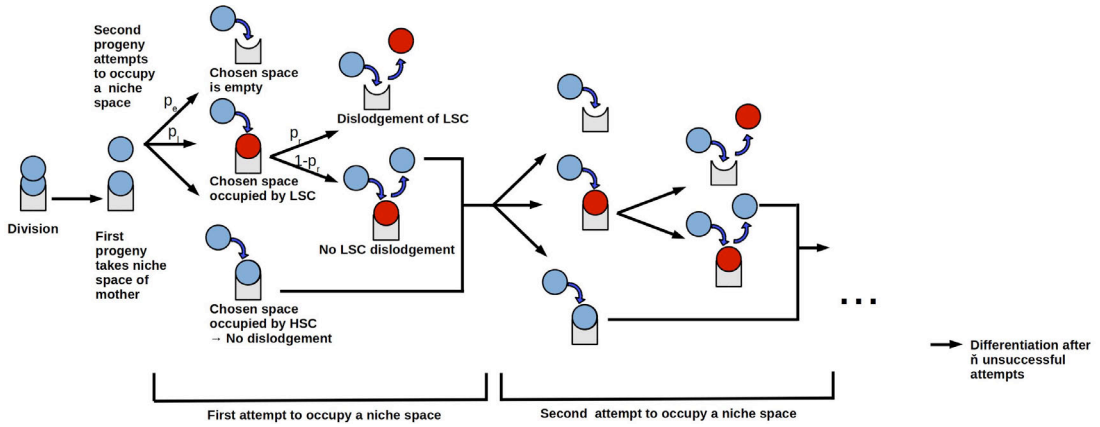

Figure S6: Overview of processes in the BM-niche.

One of the progeny cells emerging from division of a stem cell occupies the niche space of the parent cell that gave rise to it. The second progeny makes ň attempts to occupy an empty niche space or to dislodge a LSC. If this is not successful, the progeny differentiates. p_e: Probability that a niche is empty. p_l: Probability that a niche is occupied by a LSC. p_r : Probability that a LSC is dislodged by a nl-HSC.

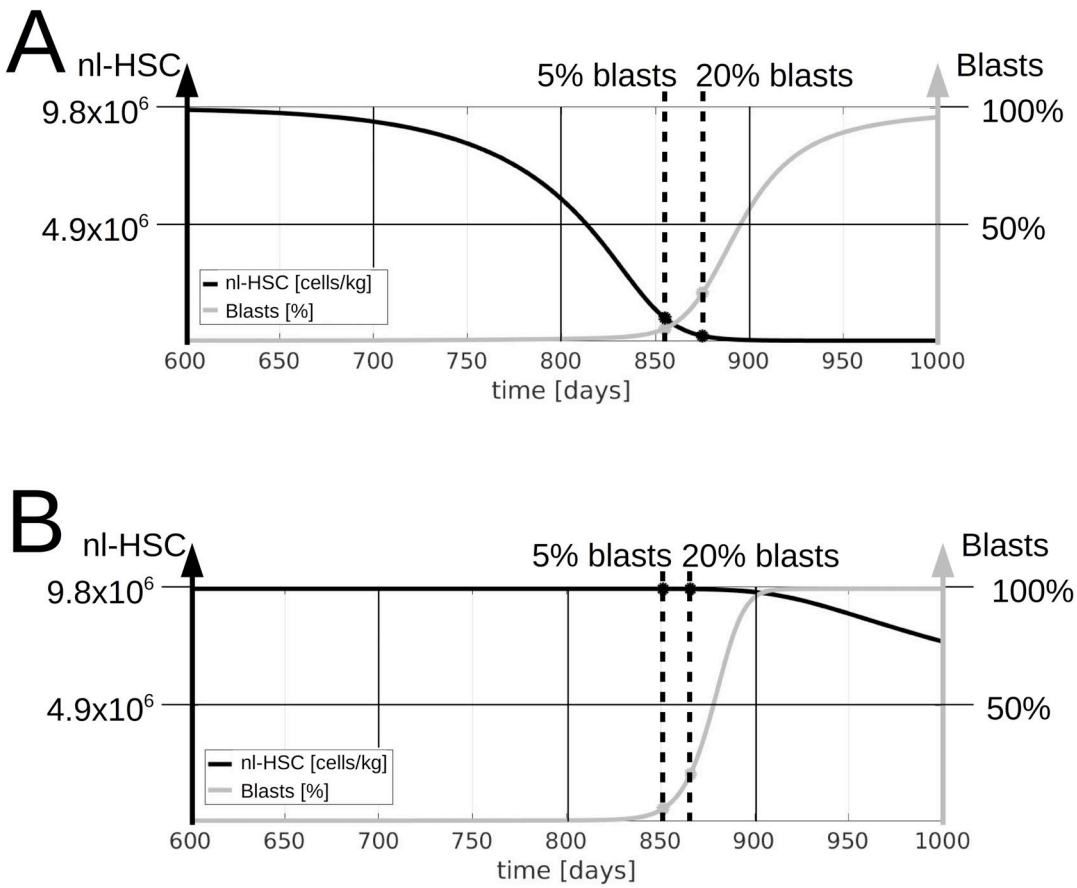

Figure S7: Model with cytokine dependent leukemic cells leads to similar dynamics as model with cytokine independent leukemic cells.

(A) Simulation of the model with cytokine dependent leukemic cells and niche competition. Also in case of cytokine dependent leukemic cells early decline of nl-HSC numbers can only be explained by a model with niche competition. (B) The mathematical model with cytokine dependent leukemic cells and without niche competition cannot reproduce the early decline of nl-HSC numbers.

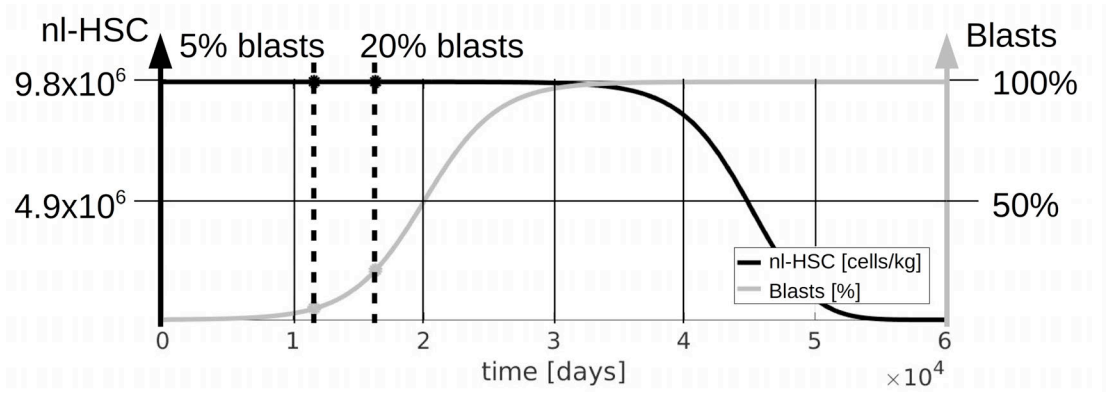

Figure S8: Niche displacement of cycling nl-HSC only is not sufficient to reproduce decline of nl-HSC before relapse.

If it is assumed that nl-HSC can only be displaced from the niche during division, the early decline of nl-HSC numbers cannot be reproduced.

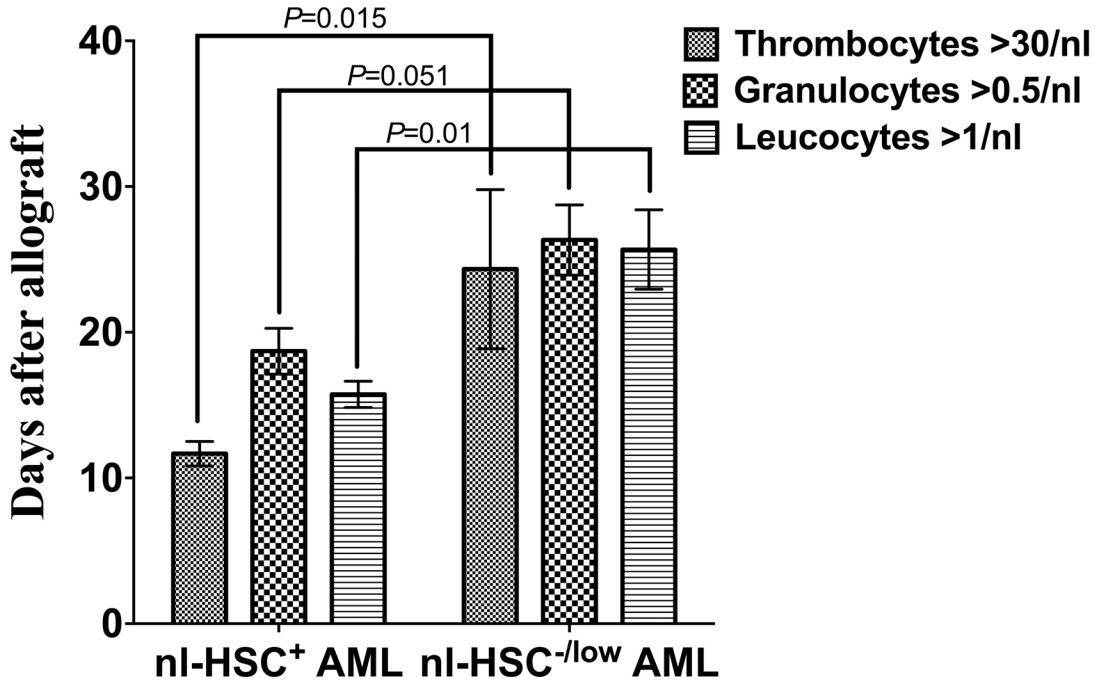

Figure S9: Allografted and relapsing nl-HSC$^{-/low}$ AML showed delayed engraftment in comparison to allografted and non-relapsing nl-HSC^{+} AML.

Comparison of median engraftment time points for thrombocytes (>30/nl), granulocytes (>0.5/nl) and leucocytes (>1/nl) of 11 nl-HSC^{+} AML and 3 nl-HSC$^{-/low}$ AML (for detailed patient information see supplementary table S5). Engraftment was significantly delayed for thrombocytes and leucocytes in nl-HSC$^{-/low}$ AML.

Supplementary Tables

Table S1: Patient characteristics.

Characteristic		nl-HSC$^-$ AML	nl-HSC$^+$ AML
n		16	45
Age years, median (range)		64.5 (48-87)	57 (27-86)
Male/ Female		13/3	25/20
Blast frequency (%), median (range)		60 (8-91)	60 (11-90)
WBC ($\times 10^9$/L), median (range)		71.34 (0.17-200.9)	13.14 (0.67-279)
Cytogenetic risk group, n (%)	Favorable	1 (6.25)	9 (20)
	Intermediate	14 (87.5)	28 (62.22)
	Adverse	1 (6.25)	8 (17.78)
***FLT3* mutation n (%)**	Positive	3 (18.75)	6 (13.33)
	Negative	10 (62.5)	31 (68.89)
	Not analyzed	3 (18.75)	8 (17.78)
***NPM1* mutation n (%)**	Positive	1 (6.25)	5 (11.11)
	Negative	13 (81.25)	35 (77.78)
	Not analyzed	2 (12.5)	5 (11.11)

Table S2: Characteristics of patients in nl-HSC tracking.

Pt	Classification	Age	Sex	Cytogenetics	Mutation			Relapse (days)	SCT (days)	Current patient status
					FLT3-ITD	*NPM1*	*CEBPa*			
1	NA	53	M	Normal	Pos	Neg	Neg	203	133	Dead, 333 days after diagnosis
2	NA	67	M	46,X,-Y,+13	Neg	Neg	Neg	73	No	Dead, 73 days after diagnosis
3	M4E0	46	M	46,XY,inv(16)	NA	Neg	NA	No	73	DF post-1st remission, 743 days after diagnosis
4	M2	59	F	47,XX,+21	Neg	Neg	Neg	No	107	DF post-SCT, 750 days after diagnosis
5	M4/5	62	F	Normal	Neg	Neg	Pos	No	No	DF post-1st remission, 1037 days after diagnosis
6	M4	63	M	Normal	Neg	Neg	Neg	No	78	DF post-SCT, 860 days after diagnosis
7	M2	48	F	45,X,-X	Neg	Pos	Neg	303	371	Dead, 383 days after diagnosis
8	M4/5	62	M	47,XY,+8	Pos	Pos	Neg	187	103	Dead, 239 days after diagnosis

9	M0	61	M	47,XY,+8	Neg	Neg	Neg	109	128	Dead, 247 days after diagnosis
10	M5	53	M	Normal	Neg	Neg	Neg	185	129	Dead, 284 days after diagnosis
11	M2 AML/ MDS	48	F	Normal	Neg	Neg	Pos	106	170	DF post-SCT, 265 days after diagnosis
14	NA	71	W	Complex	NA	Neg	NA	NA	No	Dead, 81 days after diagnosis
15	M2	67	M	Normal	Neg	Neg	NA	No	66	DF post-SCT, 397 days after diagnosis

Pt: Patient Number; SCT: stem cell transplantation; DF: disease free; NA: not available.

Table S3: Course of nl-HSC frequencies in AML patients suffering from relapse

Pt No.	Time point	Blast frequency (%)	nl-HSC frequency (%)	nl-HSC number (cells/ml)
7	Diagnosis	80	0.0027	216
	Molecular relapse	2	0.0224	358.4
	Molecular relapse	2	0.0161	241.5
8	Diagnosis	85	0.0025	700
	Molecular relapse	4	0.0134	53.6
	Frank relapse	68	0.0077	77
9	Diagnosis	90	0.0474	12798
	Frank relapse	15	0.0408	326.4
10	Diagnosis	87	0.0122	10248
	Frank relapse	8	0.0038	22.8
11	Diagnosis	53	0.002	2000
	1st Frank relapse	76	0.0035	126
	2nd Frank relapse	64	0.0026	52

Table S4: Steady state blood cell counts used for calibration of the model.

Cell Type	Cells [1/l] (ref. 22)	Cells [1/kg]*	Cells total *	Life time	dying [1/d]	Dying [1/(kg day)]*
Erythrocyte	$5 \cdot 10^{12}$	$3.1 \cdot 10^{11}$	$2.5 \cdot 10^{13}$	120 d (ref. 23)	$2.1 \cdot 10^{11}$	$2.6 \cdot 10^{9}$
Thrombocyte	$150 \cdot 10^{9}$	$9.4 \cdot 10^{9}$	$7.5 \cdot 10^{11}$	8 d (ref. 24)	$9.4 \cdot 10^{10}$	$1.2 \cdot 10^{9}$
Megakaryocyte[#]	$75 \cdot 10^{6}$	$4.7 \cdot 10^{6}$	$3.8 \cdot 10^{8}$		$4.8 \cdot 10^{7}$	$5.9 \cdot 10^{5}$
Granulocyte	$4 \cdot 10^{9}$	$2.5 \cdot 10^{8}$	$2 \cdot 10^{10}$	8h[&] (ref. 25)	$6 \cdot 10^{10}$	$7.5 \cdot 10^{8}$
Total[$]		$3.1 \cdot 10^{11}$	$2.5 \cdot 10^{13}$		$2.7 \cdot 10^{11}$	$3.4 \cdot 10^{9}$

Reference numbers refer to the Supplementary Methods.

*: assuming 5l of blood and 80 kg of body weight; [#]: Assuming that each megakaryocyte gives rise to 2000 platelets (ref. 26) we calculate to how many megakaryocytes the thrombocyte counts correspond; [&]: time in blood stream before migrating to tissue; [$]: Erythrocyte+Megakaryocyte+Granulocytes.

Table S5: Engraftment kinetics of allografted and non-relapsing nl-HSC^{+} AML versus allografted and relapsing nl-HSC$^{-/low}$ AML

Pt No.	Age	Sex	nl-HSC$^{-/low}$ (yes/no)	Relapse (yes/no)	SCT (days after diagnosis)	Conditioning regimen	Thrombocytes >30/nl (days after allograft)	Granulocytes >0.5/nl (days after allograft)	Leucocytes >1/nl (days after allograft)
3	46	M	No	No	73	TBI 8 Gy/Fludarabin	9	18	13
4	59	F	No	No	107	TBI 8 Gy/Fludarabin	11	19	14
12	32	M	No	No	77	Melphalan/Fludarabin	12	16	15
16	27	F	No	No	135	Busulfan/Fludarabin/ATG	12	17	16
17	71	F	No	No	194	Treosulfan/Fludarabin/ATG	9	24	21
18	75	M	No	No	159	Treosulfan/Fludarabin/ATG	14	19	15
19	59	F	No	No	148	Treosulfan/Fludarabin/ATG	17	24	20
20	56	M	No	No	137	Busulfan/Fludarabin	NA	25	16
21	57	F	No	No	392	Busulfan/Fludarabin	NA	17	14
22	28	F	No	No	116	Busulfan/Fludarabin/ATG	10	8	18
23	55	F	No	No	488	Melphalan/Fludarabin/ATG	11	NA	11
1	53	M	Yes	Yes	133	Treosulfan/Fludarabin/ATG	17	25	24
24	52	M	Yes	Yes	122	Melphalan/Fludarabin/ATG	35	31	31
25	65	M	Yes	Yes	104	Treosulfan/Fludarabin/ATG	21	23	22

Pt: Patient; SCT: stem cell transplantation; NA: not available.

Supplementary Methods

nl-HSC number calculation

$$\text{nl-HSC (cells/ml)} = \frac{\text{nl-HSC frequency} \times \text{MNC number after isolation (cells)}}{\text{Primary bone marrow volume after puncture (ml)}}$$

***In vivo* NOD/SCID/interleukin 2 receptor $^{\gamma null}$ (NSG) mouse transplantation**

1-2×10^6 MNC of diagnostic AML samples were T cell depleted using CD3 MicroBeads (Miltenyi, Bergisch Gladbach, Germany) according to manufacturer's instructions and subsequently transplanted by intra bone injection in sublethally irradiated (200 cGy) NSG mice. 12 to 16 weeks after transplantation animals were sacrificed and BM cells harvested. BM samples were stained with CD45-PE (clone HI30), CD33-PE-Cy7 (clone WM53) and CD19-APC (clone HIB19) (eBioscience, Frankfurt, Germany) and analyzed for AML or multi-lineage engraftment. BM samples with >0.1% human cells, defined by human CD45-positivity were scored successfully engrafted. Myeloid engraftment over 80% (human $CD33^+$ cells/human $CD45^+$ cells ≥80%) was scored AML engraftment, whereas multi-lineage engraftment was defined by myeloid and lymphoid engraftment (with $CD33^+$ cells/human $CD45^+$ cells <80% and detectable $CD19^+$ cells) Animal experiments were performed at the German Cancer Research Center (DKFZ) under institutional and governmental guidelines.

Fluorescence *in situ* hybridization (FISH) analysis

Sorted primary cells were expanded in Stemline II medium with cytokines (Sigma

Aldrich, Munich, Germany) for 7 to 10 days as described previously (ref. 14). Cells were fixed on glass slides using methanol/acetic acid (3:1, volume: volume) for 10 min. Interphase FISH analysis was performed according to the manufacturer's instructions using probes for the respective chromosome aberrations (MetaSystems, Altlussheim, Germany). Evaluation of the FISH results was performed using an automated interphase FISH spot counting system SC300-25A (Applied Spectral Imaging, Edingen-Neckarhausen, Germany). Hybridization efficiency was validated on interphase nuclei obtained from bone marrow of a healthy donor and the thresholds were set according to the threefold standard deviation.

Statistics

Statistics were performed using SPSS Statistics 19 (IBM, Armonk, NY, USA). All values are shown as mean value ± standard deviation (SD), mean value ± standard error of the mean (SEM) or median with range. Student's *t* test or Mann-Whitney U test was performed to compare differences between two groups. Kaplan-Meier-curves were used to show survival of AML patients. Differences between subgroups were calculated using log-rank test. *P* values <0.05 were considered as statistically significant.

Mathematical model

Model structure

The model describes the interaction of one hematopoietic cell lineage and one leukemic cell lineage. The hematopoietic lineage comprises 4 cell types (compartments). These are non-leukemic hematopoietic stem cells (nl-HSCs), hematopoietic progenitor cells (HPCs), hematopoietic precursor cells and post-mitotic mature blood cells. By $c_1(t)$ we denote the number of nl-HSCs per kg of body weight at time t, by $c_2(t)$, $c_3(t)$ and $c_4(t)$ we denote the respective numbers of hematopoietic progenitor cells, hematopoietic precursor cells, and mature blood cells. Details are described in the section "Parametrization of the hematopoietic system". Similarly, the leukemic cell lineage consists of leukemic stem cells (LSCs), leukemic progenitor cells, leukemic precursor cells and post-mitotic leukemic blasts. The respective leukemic cell numbers per kg of body weight at time t are denoted as $l_1(t)$, $l_2(t)$, $l_3(t)$ and $l_4(t)$.

The discrete structure of the hematopoietic system and the leukemic cells are adopted from literature (1, 2, 3, 4). Mathematical models mimicking the compartmental structure of the hematopoietic system have been successfully applied to clinically relevant questions (5, 6, 7). The presented model is an extension of the models of healthy hematopoiesis (5, 8, 9, 10) and acute leukemias (6, 11, 12). The new feature is detailed consideration of cell competition for bone marrow niche spaces including dislodgement of healthy stem cells by leukemic stem cells.

We assume that stem cells reside in a stem cell niche and can divide infinitely. In con-

trast, all mitotic non-stem cells can perform only a limited number of divisions (1, 2). The maximal number of divisions performed by progenitor cells is denoted as n_1 and that of precursor cells as n_2. A schematic overview of the structure of the hematopoietic compartment is depicted in Figure S5.

Cells are characterized by the following properties:

- **Proliferation rate p**, describing the frequency of cell divisions per unit of time. We assume that cells of the most mature compartment are post-mitotic.
- **Fraction of self-renewal a**, describing the fraction of progeny cells returning to the compartment occupied by the parent cells that gave rise to them (process referred to as self-renewal). Based on our earlier work, (8), we assume that the fraction of self-renewal is regulated by feedback-signaling.
- **Death rate d**, describing the fraction of cells dying per unit of time. For simplicity, we assume that dividing cells do not die and that non-dividing cells die at constant rates.

Feedback regulation

Formation of healthy blood cells is a tightly regulated process. If there is a need for more blood cells of a certain type, the concentration of signaling molecules (cytokines) increases and stimulates formation of mature cells (13, 14, 15). As shown by experiments (16, 17) and as in our previous models (5, 7), we assume that proliferation rates of hematopoietic stem- and progenitor cells increase with increasing cytokine stimulation. We furthermore assume that the number of divisions performed by progenitor and precursor cells before ter-

minal differentiation increases with increasing cytokine stimulation. This has been shown in (5, 8). Differentiation and self-renewal of stem cells is regulated by the niche.

We denote $s(t)$ the feedback signal regulating self-renewal of progenitor and precursor cells at time t

$$s(t) := \frac{1}{1 + kc_4(t)}, \tag{1}$$

which assumes values between zero and one. This expression can be derived from cytokine kinetics (8) and takes into account that the concentrations of important cytokines such as EPO and G-CSF depend on the concentration of mature cells (13, 15). We use the term "self-renewal" not only in the context of nl-HSCs. If a progenitor / precursor cell gives rise to progenitor / precursor cells, we also denote this as self-renewal. Importantly, in our model only stem cells have unlimited self-renewal capacity and progenitor / precursor cells differentiate after a finite number of divisions.

Self-renewal of a certain cell type at time t is assumed to be given as a maximal possible self-renewal of this cell type multiplied by $s(t)$. We denote by $a_2^c(t) := a_2^c s(t)$ the fraction of self-renewal of hematopoietic progenitors at time t. The parameter a_2^c can be interpreted as the self-renewal of progenitor cells in case of maximal cytokine stimulation. Analogously we denote by $a_3^c(t) := a_3^c s(t)$ the fraction of self-renewal of hematopoietic precursor cells at time t. In analogy the regulation of proliferation rates is modeled (5, 7) using the feedback signal

$$\tilde{s}(t) = \frac{1}{1 + \tilde{k}c_4(t)}. \tag{2}$$

The proliferation rates of hematopoietic stem and precursor cells are given by $p_i^c(t) =$

$p_i^c \tilde{s}(t)$ for $i = 1, 2$.

For simplicity, we assume for the moment that leukemic cells do not depend on cytokine signaling, due to constitutive activation of signaling pathways (18, 19, 20). This means that self-renewal and proliferation do not depend on $s(t)$ or $\tilde{s}(t)$. In the sections "Cytokine dependent leukemic cells", we present a version of the model that takes into account cytokine dependent leukemic cell expansion. Simulations of the modified model lead to similar dynamics. They are presented in Figure S7. The cytokine dependence of leukemic cells does not change the conclusions drawn from the models.

Stem cell niche

We assume that the stem cell niche has a limited capacity n_c. The niche capacity n_c is the number of stem cells per kg of body weight that can reside in the niche. We assume that stem cells dislodged from the niche differentiate into HPC. The number of empty niche spaces per kg of body weight is denoted as n_e. We treat the bone marrow niche as a 'well mixed tank'. Consequently, the probability that a randomly chosen niche space is empty is given by $p_e := n_e/n_c$. The probability that a nl-HSC occupies a randomly chosen niche space is given by $p_c := c_1/n_c$, where c_1 is the number of nl-HSCs per kg of body weight. The corresponding probability for LSC is given by $p_l := l_1/n_c$.

We assume that leukemic and hematopoietic stem cells compete for niche spaces, nl-HSCs are able to dislodge LSCs from the niche and vice versa. We denote the niche affinity of LSCs by $\eta_l \in (0, 1]$ and that of nl-HSCs by $\eta_c \in (0, 1]$. The probability that a nl-HSC dislodges a LSC is given by a function p_r^H which depends on the fraction η_c/η_l of nl-HSC and

LSC niche affinity. Precisely, the probability that a LSC is dislodged by a nl-HSC is given by $p_r^H(\eta_c/\eta_l)$. The probability that a nl-HSC is dislodged by a LSC is given by $p_r^L(\eta_l/\eta_c)$. The functions p_r^L and p_r^H are assumed to map to $[0,1]$ and to be strictly monotonously increasing with $p_r^H(0) = p_r^L(0) = 0$. We assume that dislodged stem cells differentiate into progenitor cells. We do not consider dislodgement of nl-HSC by nl-HSC and dislodgement of LSC by LSC since these do not change the size of the nl-HSC or LSC population. If we set $p_r^H \equiv 0$, the occupation of a niche space by a LSC is irreversible, i.e., a niche space occupied by a LSC at time t_0 will be occupied by a LSC for all $t > t_0$. This choice of p_r^H is compatible with the hypothesis that LSC destroy the niche space, e.g., by modification of stromal cells.

In the following, for simplicity, we set $p_r^H = p_r^L$ and denote the function by p_r. We furthermore assume that $p_r(1) = 0.5$. The latter condition implies that if cells with identical niche affinity compete for a niche space, each of the two cells has the same probability to occupy it.

For simplicity we assume that stem cells always divide symmetrically and give rise to 2 stem cells. One progeny occupies the niche space of the parent cell and maintains stemness. The second progeny makes at most $\tilde{n}$ attempts to occupy nearby niche spaces. If all $\tilde{n}$ attempts fail, the cell differentiates.

In detail the following processes are assumed to happen in the nl-HSC compartment:

- A nl-HSC divides and produces two progeny stem cells
- One progeny replaces the parent cell in its niche and thus maintains stemness

- The second progeny makes at most $\tilde{n}$ attempts to occupy a niche space

  - 1^{st} attempt: The probability that a randomly chosen niche space which the progeny tries to occupy is empty equals p_e, the probability that it is occupied by a LSC equals p_l. The probability that the LSC is dislodged equals $p_r(\eta_c/\eta_l)$. Consequently the probability that the offspring finds a niche space at the first attempt is given by

    $$p_{nicheHSC,1} := p_e + p_l p_r(\eta_c/\eta_l).$$

    The probability that a LSC is dislodged during this process equals

    $$p_{dislodgeLSC,1} = p_l p_r(\eta_c/\eta_l).$$

    The probability that the attempt to occupy a niche space is unsuccessful is given by

    $$\bar{p}_{nicheHSC,1} := 1 - p_{nicheHSC,1}.$$

  - 2^{nd} attempt: The cell makes a second attempt to occupy a niche if and only if the first attempt fails. The probability that the first attempt fails is $\bar{p}_{nicheHSC,1}$. The probability that the niche which the cell tries to occupy is empty equals p_e, the probability that it is occupied by a LSC equals p_l. The probability that the LSC is dislodged equals $p_r(\eta_c/\eta_l)$. Consequently, the probability that a nl-HSC successfully occupies a niche space during the second attempt is given by

    $$p_{nicheHSC,2} := \bar{p}_{nicheHSC,1}(p_e + p_l p_r(\eta_c/\eta_l)) = \bar{p}_{nicheHSC,1} p_{nicheHSC,1}.$$

    The probability that a LSC is dislodged during the second attempt equals

    $$p_{dislodgeLSC,2} = p_{dislodgeLSC,1} \bar{p}_{nicheHSC,1}.$$

The probability that the first and the second attempt fail equals $\bar{p}^2_{nicheHSC,1}$.

- $\tilde{n}^{th}$ attempt: The probability that the first $\tilde{n}-1$ attempts fail is given by $\bar{p}^{\tilde{n}-1}_{nicheHSC,1}$. The probability that the offspring occupies a niche during the $\tilde{n}^{th}$ attempt is given by

$$p_{nicheHSC,\tilde{n}} := \bar{p}^{\tilde{n}-1}_{nicheHSC,1}(p_e + p_l p_r(\eta_c/\eta_l)) = \bar{p}^{\tilde{n}-1}_{nicheHSC,1} p_{nicheHSC,1}.$$

The probability that a LSC is dislodged during this process is given by

$$p_{dislodgeLSC,\tilde{n}} = \bar{p}^{\tilde{n}-1}_{nicheHSC,1} p_{dislodgeLSC,1}.$$

- The probability that the second progeny cell is able to occupy a niche during at most $\tilde{n}$ subsequent attempts is given by

$$p_{lodgeHSC} := \sum_{j=1}^{\tilde{n}} p_{nicheHSC,j} = 1-(1-p_e-p_l p_r(\eta_c/\eta_l))^{\tilde{n}}.$$

- The probability that a LSC is dislodged during this process is given by

$$\begin{aligned} p_{dislodgeLSC} &= \sum_{j=1}^{\tilde{n}} p_{dislodgeLSC,j} \\ &= \begin{cases} \left(1-(1-p_e-p_l p_r(\eta_c/\eta_l))^{\tilde{n}}\right) \frac{p_l p_r(\eta_c/\eta_l)}{p_e+p_l p_r(\eta_c/\eta_l)} & \bar{p}_{nicheHSC,1} \neq 1 \\ 0 & \bar{p}_{nicheHSC,1} = 1. \end{cases} \end{aligned}$$

- The probability that the second progeny cell fails to occupy a niche during $\tilde{n}$ subsequent attempts is given by

$$p_{differentiateHSC} := 1 - p_{lodgeHSC} = \bar{p}^{\tilde{n}}_{nicheHSC,1} = (1-p_e-p_l p_r(\eta_c/\eta_l))^{\tilde{n}}.$$

The analogous processes are supposed to happen in the LSC compartment. An overview of the scenarios is given in Figure S6.

Compartment dynamics

For simplicity we neglect the duration of mitosis which is short in comparison to generation times. In the nl-HSC compartment, the flux to mitosis at time t is given by $p_1^c \tilde{s} c_1$. These cells produce $2p_1^c \tilde{s} c_1$ progeny, $p_1^c \tilde{s} c_1$ of the progeny move to the niche of their parent cells and remain stem cells. The remaining $p_1^c \tilde{s} c_1$ cells make $\tilde{n}$ attempts to find a niche space. As calculated above, in average, $(1-\bar{p}^{\tilde{n}}_{nicheHSC,1})p_1^c \tilde{s} c_1$ cells find a niche space and maintain stemness. The remaining $\bar{p}^{\tilde{n}}_{nicheHSC,1} p_1^c \tilde{s} c_1$ cells differentiate. The flux to differentiation from the nl-HSC compartment is given by the number of progeny which find no niche space and by the number of nl-HSCs which are dislodged by LSCs. The latter is given by $p_{dislodgedHSC} p_1^l l_1$. We therefore obtain:

$$
\begin{aligned}
\frac{d}{dt}c_1 = & \underbrace{-p_1^c \tilde{s} c_1}_{\text{flux to mitosis}} + \underbrace{p_1^c \tilde{s} c_1}_{\text{50\% of progeny occupy niche space of parents}} \\
& + \underbrace{p_{lodgeHSC} p_1^c \tilde{s} c_1}_{\text{progeny nl-HSC finding empty spaces or dislodging LSCs}} - \underbrace{p_{dislodgeHSC} p_1^l l_1}_{\text{nl-HSCs dislodged by dividing LSCs}} \\
= & \left(1-(1-p_e-p_l p_r(\eta_c/\eta_l))^{\tilde{n}}\right) p_1^c \tilde{s} c_1 \\
& - \begin{cases} \left(1-(1-p_e-p_c p_r(\eta_l/\eta_c))^{\tilde{n}}\right) \frac{p_c p_r(\eta_l/\eta_c)}{p_e+p_c p_r(\eta_l/\eta_c)} p_1^l l_1 & p_e + p_c p_r(\eta_l/\eta_c) \neq 0 \\ 0 & p_e + p_c p_r(\eta_l/\eta_c) = 0 \end{cases}
\end{aligned}
\tag{3}
$$

The flux from the nl-HSC compartment to differentiation is given by

$$\begin{aligned}
\nu_1^c :=& \bar{p}_{nicheHSC,1}^{\tilde{n}} p_1^c c_1 + p_{dislodgeHSC} p_1^l l_1 \\
=& (1 - p_e - p_l p_r(\eta_c/\eta_l))^{\tilde{n}} p_1^c \tilde{s} c_1 \\
&+ \begin{cases} \left(1 - (1 - p_e - p_c p_r(\eta_l/\eta_c))^{\tilde{n}}\right) \frac{p_c p_r(\eta_l/\eta_c)}{p_e + p_c p_r(\eta_l/\eta_c)} p_1^l l_1 & p_e + p_c p_r(\eta_l/\eta_c) \neq 0 \\ 0 & p_e + p_c p_r(\eta_l/\eta_c) = 0. \end{cases}
\end{aligned} \tag{4}$$

In analogy we obtain

$$\begin{aligned}
\frac{d}{dt} l_1 =& \left(1 - (1 - p_e - p_c p_r(\eta_l/\eta_c))^{\tilde{n}}\right) p_1^l l_1 \\
&- \begin{cases} \left(1 - (1 - p_e - p_l p_r(\eta_c/\eta_l))^{\tilde{n}}\right) \frac{p_l p_r(\eta_c/\eta_l)}{p_e + p_l p_r(\eta_c/\eta_l)} p_1^c \tilde{s} c_1 & p_e + p_l p_r(\eta_c/\eta_l) \neq 0 \\ 0 & p_e + p_l p_r(\eta_c/\eta_l) = 0. \end{cases}
\end{aligned} \tag{5}$$

The flux from the LSC compartment to differentiation is given by

$$\begin{aligned}
\nu_1^l =& (1 - p_e - p_c p_r(\eta_l/\eta_c))^{\tilde{n}} p_1^l l_1 \\
&+ \begin{cases} \left(1 - (1 - p_e - p_l p_r(\eta_c/\eta_l))^{\tilde{n}}\right) \frac{p_l p_r(\eta_c/\eta_l)}{p_e + p_l p_r(\eta_c/\eta_l)} p_1^c \tilde{s} c_1 & p_e + p_c p_r(\eta_l/\eta_c) \neq 0 \\ 0 & p_e + p_c p_r(\eta_l/\eta_c) = 0. \end{cases}
\end{aligned} \tag{6}$$

Progenitor cells

To account for the finite number of n_1 cell divisions a progenitor can perform, we divide the progenitor compartment into $n_1 + 1$ partitions (sub-compartments), denoted as $c_{2,0}, \ldots, c_{2,n_1}$. The second index indicates how many divisions the cells have performed

since they entered the progenitor state.

The influx from the stem cell compartment to the progenitor compartment at time t is denoted as $v_1^c(t)$. These cells enter the sub-compartment $c_{2,0}$ (sub-compartment containing all cells that have performed 0 divisions since entrance into the progenitor state). With each division the originating progenitor cells move to the next downstream sub-compartment $c_{2,1}$, $c_{2,2}$, etc.

The flux to mitosis in sub-compartment $c_{2,i}$ ($1 \leq i \leq n_1$) is given by $p_2 \tilde{s} c_{2,i}$. From mitosis $2p_2^c \tilde{s} c_{2,i}$ progeny originate. If $i < n_1$ the progeny can either be progenitors which then belong to sub-compartment $c_{2,i+1}$ or they can differentiate to the precursor state and then belong to sub-compartment $c_{3,0}$. The fraction of progeny staying in the progenitor compartment is given by $2a_2^c s p_2^c \tilde{s} c_{2,i}$, the fraction of progeny differentiating to the precursor state is given by $2(1-a_2^c s) p_2^c \tilde{s} c_{2,i}$. If cells from sub-compartment c_{2,n_1} divide, all $2p_2^c \tilde{s} c_{2,n_1}$ progeny move to the precursor state $c_{3,0}$. This results in the following set of equations:

$$
\begin{aligned}
\frac{d}{dt} c_{2,0} &= \underbrace{v_1^c}_{\text{influx from nl-HSCs}} - \underbrace{p_2^c \tilde{s} c_{2,0}}_{\text{flux to mitosis}} \\
\frac{d}{dt} c_{2,1} &= \underbrace{2a_2^c s p_2^c \tilde{s} c_{2,0}}_{\text{influx from } c_{2,0}} - \underbrace{p_2^c \tilde{s} c_{2,1}}_{\text{flux to mitosis}} \\
&\vdots \\
\frac{d}{dt} c_{2,n_1} &= \underbrace{2a_2^c s p_2^c \tilde{s} c_{2,n_1-1}}_{\text{influx from } c_{2,n_1-1}} - \underbrace{p_2^c \tilde{s} c_{2,n_1}}_{\text{flux to mitosis}}
\end{aligned}
\tag{7}
$$

The influx ν_2^c to the precursor compartment is given by (i) cells that have differentiated without having performed the maximal number of divisions and (ii) cells differentiating having performed the maximal number of n_1 divisions in the progenitor compartment. Therefore, $\nu_2^c(t) = 2p_2^c\tilde{s}c_{2,n_1} + 2\big(1-a_2^c s\big)p_2^c\tilde{s}\sum_{i=0}^{n_1-1} c_{2,i}$. A similar system of equations has been derived in ref. (10).

The equations for the leukemic progenitor cells are obtained analogously. The only difference is, that leukemic cells do not depend on feedback mechanisms.

$$\begin{aligned}
\frac{d}{dt}l_{2,0} &= \underbrace{\nu_1^l}_{\text{influx from LSCs}} - \underbrace{p_2^l l_{2,0}}_{\text{flux to mitosis}} \\
\frac{d}{dt}l_{2,1} &= \underbrace{2a_2^l p_2^l l_{2,0}}_{\text{influx from } l_{2,0}} - \underbrace{p_2^l l_{2,1}}_{\text{flux to mitosis}} \\
&\vdots \\
\frac{d}{dt}l_{2,n_1} &= \underbrace{2a_2^l p_2^l l_{2,n_1-1}}_{\text{influx from } l_{2,n_1-1}} - \underbrace{p_2^l l_{2,n_1}}_{\text{flux to mitosis}}
\end{aligned} \tag{8}$$

The influx ν_2^l to the precursor compartment is given by $\nu_2^l(t) = 2p_2^l l_{2,n_1} + 2\big(1-a_2^l\big)p_2^l\sum_{i=0}^{n_1-1} l_{2,i}$.

Precursor cells

We assume that precursor cells can perform at most n_2 divisions. The equations describing dynamics of the precursor compartments are obtained in analogy to the equations describ-

ing progenitor dynamics. The only difference is that proliferation rate of hematopoietic precursors is assumed to be constant, as suggested by experimental data (16, 17). We obtain:

$$\begin{aligned}
\frac{d}{dt}c_{3,0} &= \nu_2^c - p_3^c c_{3,0} \\
\frac{d}{dt}c_{3,1} &= 2a_3^c s p_3^c c_{3,0} - p_3^c c_{3,1} \\
&\vdots \\
\frac{d}{dt}c_{3,n_2} &= 2a_3^c s p_3^c c_{3,n_2-1} - p_3^c c_{3,n_2} \\
\frac{d}{dt}l_{3,0} &= \nu_2^l - p_3^l l_{3,0} \\
\frac{d}{dt}l_{3,1} &= 2a_3^l p_3^l l_{3,0} - p_3^l l_{3,1} \\
&\vdots \\
\frac{d}{dt}l_{3,n_2} &= 2a_3^l p_3^l l_{3,n_2-1} - p_3^l l_{3,n_2}.
\end{aligned} \tag{9}$$

The influx ν_3^c to the post-mitotic cell compartment is given by

$$\nu_3^c(t) = 2p_3^c c_{3,n_2} + 2\big(1 - a_3^c s\big) p_3^c \sum_{i=0}^{n_2-1} c_{3,i}$$

$$\nu_3^l(t) = 2p_3^l l_{3,n_2} + 2\big(1 - a_3^l\big) p_3^l \sum_{i=0}^{n_2-1} l_{3,i}.$$

Post-mitotic cells

The post-mitotic cells of the hematopoietic and leukemic cell line die at constant rates. The death rate for mature hematopoietic cells is denoted as d_4^c, that of post-mitotic leukemic

cells as d_4^l. We obtain the following equations:

$$\begin{aligned}\frac{d}{dt}c_4 &= \nu_3^c - d_4^c c_4 \\ \frac{d}{dt}l_4 &= \nu_3^l - d_4^l l_4.\end{aligned} \tag{10}$$

ODE system

The full model is given by the ordinary differential equations (3)-(10) together with the feedback signals from equations (1) and (2) and $p_c \equiv p_c(t) = c_1(t)/n_c$, $p_l \equiv p_l(t) = l_1(t)/n_c$ and $p_e \equiv p_e(t) = 1 - p_c(t) - p_l(t)$. The function p_r is monotonously increasing and fulfills $p_r(0) = 0$, $p_r(1) = 0.5$, $p_r(\infty) = 1$. We assume that the initial conditions are non-negative and fulfill $c_1(0) + l_1(0) \leq n_c$.

Parametrization of the hematopoietic system

Mature cell counts

We assume an average body weight of 80 kg and a blood volume of 5 liters. We denote the steady state count of mature cells as $\bar{c}_4$. We calibrate $\bar{c}_4$ based on physiological healthy blood cell counts and physiological life spans of the individual cell types. We do not consider lymphocytes which proliferate and mature in the lymphatic tissues (21). Platelets are formed out of megakaryocytes by a fragmentation process that is different from mitosis. We do not model the process of thrombocyte formation in detail. Instead we consider megakaryocytes and not thrombocytes in the model. Megakaryocytes originate from the stem cells by proliferation and differentiation similarly as the other mature cell types. Ma-

ture cell counts are summarized in Table S4. Based on the values from the Table S4, we have $\bar{c}_4 = 3.1 \cdot 10^{11}$ mature cells per kg of body weight.

nl-HSC and progenitor counts

We identify the $CD34^+CD38^-ALDH^+$ cells with nl-HSCs and $CD34^+CD38^+ALDH^+$ cells with hematopoietic progenitors. Our measurements in healthy subjects imply that in average 0.098% of mono-nucleated cells (MNC) are nl-HSC and 0.251% of MNC are progenitors. The estimations of nucleated cells per kg of body weight reach from 10^{10} to $\approx 3.5 \cdot 10^{10}$ per kg (27, 28, 29). Since 20-30% of nuclear cells are considered to be MNC (30), we assume that we have approximately 10^{10} MNC per kg of body weight. Then we obtain as steady state nl-HSC count $\bar{c}_1 = 9,8 \cdot 10^6$ cells per kg of body weight and as progenitor count $\bar{c}_2 = 2.5 \cdot 10^7$ cells per kg of body weight.

Division rates

It is known from experiments that division rates of stem and progenitor cells can increase at most 4 fold (16). Based on literature, it is known that stem cells divide approximately twice per year in equilibrium (corresponding to a proliferation rate of $3.8 \cdot 10^{-3}/day$) (31). Since the maximal proliferation rate is 4 times higher, we set $p_1^c = 15.2 \cdot 10^{-3}/day$. We assume that precursors divide approximately once per day ($p_3 = 0.69/day$). This is in accordance with data from granulopoiesis and with model based parameter estimations for erythropoiesis, (5, 7, 32, 33). It is known that with increasing amounts of CD38 expression division frequency increases. In peripheral stem cell grafts progenitor cell cycle durations between 1 day and 10 days have been reported, (34). For simplicity we assume a steady state division frequency of once per week (corresponding to a proliferation rate of $0.1/day$),

the 4 fold increased maximal rate is then $p_2^c = 0.4/day$.

Death rates

We assume that immature cells do not die. Based on the data from Table S4, we calculate the average death rate for the mature cells. We obtain $d_n \approx 10^{-2}/day$.

Parameter $\tilde{k}$

We denote $\bar{\tilde{s}}$ the steady state value of $\tilde{s}$. It is known from experiments that division rates of immature cells can increase at most 4 fold compared to steady state values (16). Therefore, $\bar{\tilde{s}} = 0.25$. We choose $\tilde{k}$ such that $\frac{1}{1+\tilde{k}\bar{c}_4} = \bar{\tilde{s}}$. Then we can calculate $\nu_1^c = \bar{c}_1 p_1^c \bar{\tilde{s}}$.

Further parameters

The other parameters follow from a computational calibration process. They are not unique. Nevertheless, simulation results are similar for the different parameter sets obtained. The calibration process is based on analytical calculation of the steady states. We express all unknown parameters as a function of known parameters, steady state cell counts and a_2, n_1, n_2. On this three dimensional manifold we search for parameter sets leading to realistic engraftment kinetics after stem cell transplantation (at least $5 \cdot 10^8$ neutrophils per liter of blood 2 weeks after transplantation of a standard dose of $CD34^+$ cells) (35).

Simulation results

The simulations shown in the main text and in Figures S7 and S8 are obtained by setting $n_1 = 30$, $n_2 = 20$, $n_c = \bar{c}_1$, $\tilde{n}$=5, $a_1^c = 1$, $a_2^c = 0.57303$, $a_3^c = 0.73994$, $k = 2.9222 \cdot 10^{-13}$,

$\tilde{k} = 9.6 \cdot 10^{-12}$, $a_1^l = 1$, $a_2^l = a_2^c$, $a_3^l = a_3^c$, $p_1^l = 5p_1^c$, $p_2^l = p_2^c$, $p_3^l = p_3^c$, $d_4^l = d_4^c$, $\eta_l/\eta_c = 400$. Other parameter sets obtained from the calibration procedure lead to similar results. We set $p_r(x) = \frac{1}{1+x}$. This implies that if two cells have the same niche affinity, the probability that one of them dislodges the other is 50%. To simulate cytokine dependent leukemic cells (see sections "Cytokine dependent leukemic cells") we set $\tilde{m} = \tilde{k}$ and $m = k$. Different choices lead to similar results. The smaller a_2^l and a_3^l and the higher p_1^l, the later the blast count increases in comparison the decline of nl-HSC. As initial condition we set healthy steady state cell counts and one leukemic stem cell.

Simulations show that the nl-HSC count at diagnosis decreases with increasing value of η_l/η_c. This observation leads to the conclusion that niche affinity of LSC is higher in nl-HSC$^{-/low}$ AML compared to nl-HSC^{+} AML.

Cytokine dependent leukemic cells

So far, we have assumed that the leukemic cells do not depend on cytokine signaling. At least for some patients, this assumption might be invalid. The following findings underline the importance of cytokines for leukemic cell expansion: (i) Leukemic blasts of some patients do no expand in vitro in absence of cytokines ref. (36, 37), (ii) leukemic cells of some patients express cytokine receptors, ref. (38), and show enhanced expansion in response to cytokine stimulation ref. (39, 40), (iii) NOD/SCID mice transgenic for human growth factors show improved engraftment of human AML samples compared to conventional NOD/SCID mice ref. (41, 42, 43).

In this section, we provide a version of the model that takes into account the dependence

of leukemic cells on hematopoietic cytokines. We assume that the cytokines have similar effects on healthy and leukemic cells. As above and in accordance with ref. (6, 11), we assume that increased cytokine concentrations lead to increased proliferation rates of leukemic stem and progenitor cells. We furthermore assume that the number of divisions performed by leukemic cells in the progenitor and precursor state increases with increasing cytokine stimulation.

Similar as in ref. (6, 11), we set

$$s(t) := \frac{1}{1 + kc_4(t) + ml_4(t)}, \tag{11}$$

and

$$\tilde{s}(t) = \frac{1}{1 + \tilde{k}c_4(t) + \tilde{m}l_4(t)}, \tag{12}$$

to take into account binding of cytokines to receptors on leukemic cells. The signal $\tilde{s}(t)$ regulates proliferation of healthy and leukemic stem- and progenitor cells. The signal $s(t)$ regulates the number of divisions performed in the progenitor and precursor compartments of healthy and leukemic cells. The full model is given by equations (3)-(10) with p_1^l, p_2^l substituted by $p_1^l\tilde{s}(t)$, $p_2^l\tilde{s}(t)$ and a_2^l, a_3^l substituted by $a_2^l s(t)$, $a_3^l s(t)$. The signals $\tilde{s}(t)$ and $s(t)$ are given by equations (11) and (12). A simulation of this model is depicted in Figure S7. Simulation results are very similar to the scenario with cytokine independent leukemic cells. Also in case of cytokine dependent leukemic cells, the decline of nl-HSC before overt leukemia can only be observed in presence of niche competition and nl-HSC dislodgement.

Dislodgement during division

So far we have assumed that each nl-HSC can be dislodegd by a LSC and, with a smaller probability, vice versa. An alternative scenario could be that cells detach from the niche during division and that only detached cells can be dislodged. This means that LSCs can only occupy niches of dividing nl-HSCs and vice versa. We can model this scenario by adjusting the quantities p_c and p_l. As defined above, p_c is the probability that a randomly chosen niche space contains a nl-HSC that is a potential candidate to be dislodged by a LSC, p_l is defined analogously. In the section "Stem cell niche", we have set $p_c(t) := c_1(t)/n_c$, where $c_1(t)$ is the number of nl-HSCs per kg of body weight at time t and n_c the number of niche spaces per kg of body weight. This choice implies that all nl-HSCs, independent of their cycling status, are candidates for potential dislodgement. To allow that only cells during division are candidates for dislodgement, we set $p_c(t) := c_{1,div}(t)/n_c$, where $c_{1,div}(t)$ is the number of nl-HSCs per kg of body weight that are in mitosis at time t. The flux of nl-HSCs to mitosis at time t is given by $p_1^c \tilde{s}(t) c_1(t)$. If we assume that τ_m is the average duration of mitosis, we obtain $c_{1,div}(t) = \int_{t-\tau_m}^{t} p_1^c \tilde{s}(\theta) c_1(\theta)\, d\theta$. We can approximate this quantity by $p_1^c \tilde{s}(t) c_1(t) \tau_m$. In analogy we define $l_{1,div}(t) = \int_{t-\tau_m}^{t} p_1^l l_1(\theta)\, d\theta \approx p_1^l l_1(t) \tau_m$ and $p_l(t) := l_{1,div}(t)/n_c$. We simulated the model with these modifications and for $\tau_m \in [0.5\ day,\ 5\ days]$. An example simulation ($\tau_m = 1\ day$) is depicted in Figure S8. Simulation results imply that if only mitotic cells can be dislodged from their niche, the early decline of nl-HSCs is not observed. Furtermore the time between appearance of the first LSC and clinical onset of the disease is prolonged.

Model without niche competition

To study the impact of niche competition on the nl-HSC population, we compare simulations of the model described above to simulations of a model without niche competition. To design a model without niche competition, we assume that nl-HSC and LSC reside in different niches. To observe decline of healthy blood cell counts it is necessary that leukemic and healthy cells interact. In accordance with previous models on acute leukemias we assume in this model that leukemic cells induce differentiation in all types of healthy cells (6). This mode of interaction corresponds to a competition between healthy and leukemic cells that is not confined to the niche space but to all hematopoietic cell types. This interaction could be mediated by cytokines or other soluble signaling molecules (6).

For simplicity we assume that both the niche for nl-HSC and the niche for LSC have the same capacity n_c. Interaction between healthy and leukemic cells is realized using a signal $\hat{s}(t) = \frac{1}{1+\hat{k}\left(l_1(t)+\sum_{i=0}^{n_1} l_{2,i}(t)+\sum_{i=0}^{n_2} l_{3,i}(t)+l_4(t)\right)}$. We assume that self-renewal of hematopoietic cells decreases in presence of leukemic cells. For this purpose we set $a_1^c(t) = 1 \cdot \hat{s}(t)$, $a_2^c(t) = a_2 \cdot \hat{s}(t)s(t)$ etc. This kind of feedback has been established in previous models of acute leukemias and has widely been used (6, 11, 12). Since the niches are separated, we obtain $p_e = (n_c - c_1)/n_c$ and p_l=0 for the nl-HSC niche (no LSCs are residing in the nl-HSC niche). and $p_e = (n_c - l_1)/n_c$ and p_c=0 for the LSC niche (no nl-HSCs are residing in the LSC niche).

These assumptions result in the following equations for c_1 and l_1:

$$\frac{d}{dt}c_1 = \underbrace{-p_1^c \tilde{s} c_1}_{\text{flux to mitosis}} + \underbrace{\hat{s} p_1^c \tilde{s} c_1}_{\text{with prob. } \hat{s} \text{ one progeny takes parents' niche}} + \underbrace{\left(1 - \left(1 - \frac{n_c - c_1}{n_c}\right)^{\tilde{n}}\right) a_1^c \hat{s} p_1^c \tilde{s} c_1}_{\text{progeny nl-HSC finding empty spaces}}$$

$$\frac{d}{dt}l_1 = \underbrace{-p_1^l l_1}_{\text{flux to mitosis}} + \underbrace{p_1^l l_1}_{\text{one progeny occupies niche of parents}} + \underbrace{\left(1 - \left(1 - \frac{n_c - l_1}{n_c}\right)^{\tilde{n}}\right) p_1^l l_1}_{\text{progeny LSC finding empty spaces}} \tag{13}$$

The other equations are analogous to the equations presented above. The only modification is that self-renewal of hematopoietic cells depends in this model also on $\hat{s}$, i.e., $a_i^c(t) = a_i^c s\hat{s}$. For the simulations depicted in the main text we take parameters from the section "Simulation results" and set $\hat{k} = 2.9 \cdot 10^{-11}$. Simulation results remain qualitatively unchanged for $\hat{k}$ varying over several orders of magnitude. Simulating modifications of the model where $\hat{s}$ only depends on post-mitotic leukemic cells or only on LSC leads to comparable results. Similarly, the models from ref. (11) and ref. (12) which assume a competition of healthy and leukemic cells for cytokines or increased death rates of immature hematopoietic cells in presence of leukemia, cannot reproduce the early decline of nl-HSC. This provides evidence that niche competition together with nl-HSC dislodgement is required to explain the observed decrease of nl-HSC counts before overt relapse.

Cytokine dependent leukemic cells

Cytokine dependent expansion of leukemic cells can be included in the model without niche competition. As above, we assume that increased cytokine concentrations lead to increased proliferation rates of leukemic stem/progenitor cells and that the number of divisions in the progenitor/precursor state increases with increasing cytokine stimulation. The modified

model is obtained from the model without niche competition with p_1^l, p_2^l substituted by $p_1^l \tilde{s}(t)$, $p_2^l \tilde{s}(t)$ and a_2^l, a_3^l substituted by $a_2^l s(t)$, $a_3^l s(t)$. The signals $\tilde{s}(t)$ and $s(t)$ are given by equations (11) and (12). A simulation of this model is depicted in Figure S7 (B). The model with cytokine dependent leukemic cells and without niche competition cannot reproduce the early decline of nl-HSC observed in the data.

References

(1) Jandl JH. Blood cell formation. In: Jandl JH, editor. Textbook of Hematology. Boston, MA: Littel Brown and Company; 1996. p. 1-69.

(2) Kipps TJ. The organization and structure of lymphoid tissues. In: Kaushansky K, Lichtman M, Beutler E, Kipps T, Seligsohn U, Prchal J, editors. Williams Hematology, 8th ed., New York: Mc Graw Hill, 2010, p. 75–84.

(3) Bonnet D, Dick JE. Human acute myeloid leukemia is organised as a hierarchy that originates from a primitive hematopoietic cell. Nat Med. **1997**; 3: 730-7.

(4) Hope KJ, Jin L, Dick JE. Acute Myeloid leukemia originates from a hierarchy of leukemic stem cell classes that differ in self-renewal capacity. Nat Immunology. **2004**; 5: 738-43.

(5) Stiehl T, Ho AD, Marciniak-Czochra A. The impact of CD34+ cell dose on engraftment after SCTs: personalized estimates based on mathematical modeling. Bone Marrow Transplant. **2014**; 49: 30–7.

(6) Stiehl T, Baran N, Ho AD, Marciniak-Czochra A. Cell division patterns in acute myeloid leukemia stem-like cells determine clinical course: a model to predict patient survival. Cancer Res. **2015**; 75: 940-9.

(7) Stiehl T, Ho AD, Marciniak-Czochra A. Assessing hematopoietic (stem-) cell behavior during regenerative pressure Adv Exp Med. **2014**; 844: 940-9.

(8) Marciniak-Czochra A, Stiehl T, Jäger W, Ho AD, Wagner W. Modeling of asymmetric cell division in hematopoietic stem cells – regulation of self-renewal is essential for efficient repopulation. Stem Cells Dev. **2009**; 18: 377–385.

(9) Stiehl T, Marciniak-Czochra A. Characterization of stem cells using mathematical models of multistage cell lineages. Mathematical and Computer Modelling **2011**; 53: 1505-17.

(10) Marciniak-Czochra A, Stiehl T, Wagner W. Modeling of replicative senescence in hematopoietic development. Aging (Albany NY) **2009**; 1: 723-32.

(11) Stiehl T, Marciniak-Czochra A. Mathematical modelling of leukemogenesis and cancer stem cell dynamics. Math Mod Natural Phenomena. **2012**; 7: 166-202.

(12) Stiehl T, Baran N, Ho AD, Marciniak-Czochra A. Clonal selection and therapy resistance in acute leukaemias: mathematical modelling explains different proliferation patterns at diagnosis and relapse. J R Soc Interface. **2014**; 11:20140079.

(13) Layton JE, Hockman H, Sheridan WP, Morstyn G. 1989 Evidence for a novel in vivo control mechanism of granulopoiesis: mature cell-related control of a regulatory growth factor. Blood **1989**; 74: 1303-7.

(14) Metcalf D. Hematopoietic cytokines. Blood **2008**; 111: 485-91.

(15) Fried W. Erythropoietin and erythropoiesis. Exp Hematol. **2009**; 37: 1007-15.

(16) Thornley I, Sutherland DR, Nayar R, Sung L, Freedman MH, Messner HA. Replicative stress after allogeneic bone marrow transplantation: changes in cycling of CD34+CD90+ and CD34+CD90- hematopoietic progenitors. Blood **2001**; 97: 1876-1878.

(17) Craig W, Kay R, Cutler R, Lansdorp PM. Expression of Thy-1 on human hematopoietic progenitor cells. J Exp Med. **1993** 177: 1331-1342.

(18) Hayakawa F, Towatari M, Kiyoi H, Tanimoto M, Kitamura T, Saito H, et al. Tandem-duplicated Flt3 constitutively activates STAT5 and MAP kinase and introduces autonomous cellgrowth in IL-3-dependent cell lines. Oncogene **2000**; 19: 624-631.

(19) Polak R, Buitenhuis M. The PI3K/PKB signaling module as key regulator of hematopoiesis: implications for therapeutic strategies in leukemia. Blood **2012**; 119: 911-923.

(20) Reilly J. FLT3 and its role in the pathogenesis of acute myeloid leukaemia. Leuk Lymphoma. **2003**; 44: 1-7.

(21) Smith, C. Production, distribution and fate of neutrophils. In: Kaushansky K, Lichtman M, Beutler E, Kipps T, Seligsohn U, Prchal J, editors. Williams Hematology, 8th ed., New York: Mc Graw Hill, 2010, p. 11–24.

(22) Ryan, DH. Examination of Blood cells. In: Kaushansky K, Lichtman M, Beutler E, Kipps T, Seligsohn U, Prchal J, editors. Williams Hematology, 8th ed., New York: Mc Graw Hill, 2010, p. 891–896.

(23) Franco RS. Measurement of Red Cell Lifespan and Aging. Transfus Med Hemother. **2012**; 39: 302-307.

(24) Harker LA, Roskos LK, Marzec UM, Carter RA, Cherry JK, Sundell B, et al. 2000 Effects of megakaryocyte growth and development factor on platelet production, platelet life span, and platelet function in healthy human volunteers. Blood **2000**; 95: 2514-22.

(25) Cartwright GE, Athens JW, Wintrobe MM. The kinetics of granulopoiesis in normal man. Blood **1964**; 24: 780–803.

(26) Kaufman RM, Airo R, Pollack S, Crosby WH. Circulating megakaryocytes and platelet release in the lung. Blood **1965**; 26: 720-731

(27) Osgood, EE. Number and distribution of human hemic cells. Blood **1954**; 9: 1141-1154.

(28) Harrison, WJ. The total cellularity of the bone marrow in man. J Clin Pathol. **1962**; 15: 254–259.

(29) Skarberg KO. Cellularity and cell proliferation rates in human bone marrow I - An in Vivo Method to Estimate the Total Marrow Cellularity in Man. Acta Medica Scandinavica **1974**; 195: 291-299.

(30) Goldstein J, Biotechnology of Blood (Biotechnology Series 19), Butterworth Heinemann, Boston, 1987.

(31) Shepherd BE, Guttorp P, Lansdorp PM, Abkowitz JL Estimating human hematopoietic stem cell kinetics using granulocyte telomere lengths. Exp Hematol. **2004**; 32: 1040–1050.

(32) Cronkite EP. Kinetics of granulopoiesis. Clin Haematol. **1979**; 8: 351–370.

(33) Fuertinger D, Kappel F, Thijssen S, Levin N, Kotanko P. A model of erythropoiesis in adults with sufficient iron availability. J Math Biol. **2013**; 66: 1209–40.

(34) Holm M, Thomsen M, Hoyer M, Hokland P. Dynamic cell cycle kinetics of normal CD34+ cells and CD38+/- subsets of haemopoietic progenitor cells in G-CSF-mobilized peripheral blood. Br J Haematol. **1999**; 105: 1002-1013.

(35) Klaus J, Herrmann D, Breitkreutz I, Hegenbart U, Mazitschek U, Egerer G, et al. Effect of CD34 cell dose on hematopoietic reconstitution and outcome in 508 patients with multiple myeloma undergoing autologous peripheral blood stem cell transplantation. Eur J Haematol. **2007**; 78: 21–28.

(36) Reilly IA, Kozlowski R, Russell NH. Heterogeneous mechanisms of autocrine growth of AML blasts. Br J Haematol. **1989**; 72: 363-369.

(37) Hunter AE, Rogers SY, Roberts IA, Barrett AJ, Russell N. Autonomous growth of blast cells is associated with reduced survival in acute myeloblastic leukemia. Blood **1993**; 82: 899-903.

(38) Kondo S, Okamura S, Asano Y, Harada M, Niho Y. Human granulocyte colony-stimulating factor receptors in acute myelogenous leukemia. Eur J Haematol. **1991**; 46: 223-30.

(39) Vellenga E, Ostapovicz D, O'Rourke B, Griffin JD. Effects of recombinant IL-3, GM-CSF, and G-CSF on proliferation of leukemic clonogenic cells in short-term and long-term cultures. Leukemia **1987**; 1: 584-589.

(40) Tsuzuki M, Ezaki K, Maruyama F, Ino T, Kojima H, Okamoto M, et al. Proliferative effects of several hematopoietic growth factors on acute myelogenous leukemia cells and correlation with treatment outcome. Leukemia **1997**; 11: 2125-2130.

(41) Feuring-Buske M, Gerhard B, Cashman J, Humphries RK, Eaves CJ, Hogge DE. Improved engraftment of human acute myeloid leukemia progenitor cells in beta 2-microglobulin-deficient NOD/SCID mice and in NOD/SCID mice transgenic for human growth factors. Leukemia **2003**; 17: 760-763.

(42) Wunderlich M, Chou FS, Link KA, Mizukawa B, Perry RL, Carroll M, et al. AML xenograft efficiency is significantly improved in NOD/SCID-IL2RG mice constitutively expressing human SCF, GM-CSF and IL-3. Leukemia **2010**; 24: 1785-1788.

(43) Ellegast JM, Rauch PJ, Kovtonyuk LV, Mueller R, Wagner U, Saito Y, et al. inv(16) and NPM1mut AMLs engraft human cytokine knock-in mice. Blood **2016**; 128: 2130-2134.